Refinement of Insulator-based Dielectrophoresis

Claire V. Crowther & Mark A. Hayes

Arizona State University, School of Molecular Sciences

Corresponding Author:
Dr. Mark A. Hayes
Arizona State University
Department of Chemistry and Biochemistry
Mail Stop 1604
Tempe AZ 85287
mhayes@asu.edu
Ph. (480) 965-2566, FAX (480) 965-2747

Abbreviations: dielectrophoresis (DEP), insulator-based dielectrophoresis (iDEP), gradient insulator-based dielectrophoresis (g-iDEP), electrophoresis (EP), electroosmosis (EO), electrokinetic mobility (μ_{EK}), electrophoretic mobility (μ_{EP}), electroosmotic mobility (μ_{EO}), dielectrophoretic mobility (μ_{DEP}), Clausius-Mossotti factor (f_{CM}), electrokinetic velocity ($\vec{v}_{EK}$) dielectrophoretic velocity ($\vec{v}_{DEP}$), electric field strength ($\vec{E}$), dielectrophoretic gradient factor ($\nabla\left|\vec{E}\right|^2$)

Keywords (max 5): dielectrophoresis, electrophoresis, trapping, efficiency, electrokinetics

Total Words (excluding title page): 5,336

Abstract

The ability to separate analytes with increasingly similar properties drives the field of separation science. One way to achieve such separations is using trapping and streaming dielectrophoresis (DEP) which directly exploits the subtle differences in electrophysical properties of analytes. The non-uniform fields necessary for DEP can be formed using various insulator shapes in microchannels. Current insulator shapes include triangles, diamonds, circles, and rectangles. However, all of these insulators pose problems for trapping, streaming, and sorting (deflection) as they are not behaviorally consistent across the lateral dimension. This leads to analytes experiencing different forces depending on their pathline in the microchannel and result in low resolution separations. Based on an iterative process testing approximately 40 different insulator shapes, a design was developed that improves particle streamlines, trapping efficiency, and induces laterally similar environments. The design was assessed by calculating and plotting the electric field, gradient of the electric field squared, and the ratio of the two. The improved design includes a unique new multi-length scale element. The multi-length scale structure streamlines the analyte(s) and improves homogeneity in the lateral dimension, while still achieving high gradients necessary for analyte separation using DEP. The design improves resolution and essentially eliminates extraneous trapping zones.

Introduction:

In the last several years the exploitation of microfluidics as a method for analyte manipulation has grown rapidly; particularly for biological samples. This is driven by the current limitations of diagnostic methods, especially the need for large sample volumes, lengthy analysis time, and low resolution/sensitivity. Microfluidic devices have the potential to improve each of these figures of merit and provide for easy portability and the use on a wide range of analytes including bioparticles. Among the latter class: animal cells[1], organelles[2], proteins[3,4], DNA[5-7] and bacteria[8-11] have been probed.

One major division of microfluidics uses electrokinetic (EK) and the dielectrophoretic (DEP) forces on particles (molecules are considered particles for the purposes of this discussion). The EK forces allows for the manipulation of both the particle and the suspending medium, as it is the sum of electrophoresis and electroosmosis. DEP is the force that is exerted on a polarizable particle present in a non-uniform electric field ($\vec{E}$). Utilizing EK and DEP forces, trapping and streaming of particles is possible. This allows for the separation of analytes bases on their specific and subtle electrical properties.[10, 12-14]

Previous work on DEP separations has utilized electrode-based dielectrophoresis (eDEP) for separations, which has the advantage of being able to induce high field gradients with a low applied voltage.[6, 15-17] Fabrication of eDEP devices is difficult and expensive, which is made worse as electrodes are easily fouled, rendering the channels non-reusable. The electrodes cause further issues as electrolysis creates bubbles and the high gradients are only local to the electrodes. Insulator-based dielectrophoresis (iDEP) is an alternative to induce non–uniform electric fields in a microchannel. In contrast to eDEP, the electrodes are placed in distal inlet and outlet reservoirs and the electric field is defined by channel insulators and the conductive media.

This resolves many of the issues encountered with eDEP (electrolysis, bubbles, fouling). Both AC and DC fields can be used with iDEP; DC fields drive overall particle movement since it induces EK and DEP transport and AC can refine separations influencing DEP only.[16, 18] iDEP was theoretically conceived and proof of concept established in the early 2000s.[6,19] Since then many different types of insulators have been utilized to achieve points of constriction[15] including single obstacles of various shapes[20,21], oil menisci[22,23], and insulating posts.[19, 24-26] The first separation to be demonstrated using iDEP was that of live and dead bacteria.[9, 10]

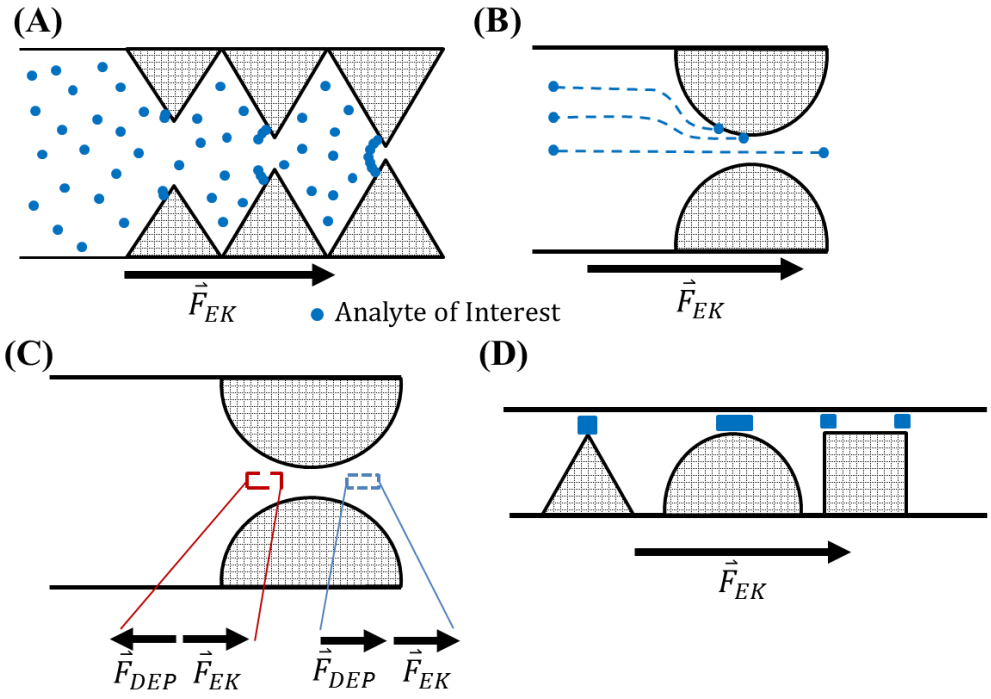

Figure 1. General illustration showing similar physical processes regardless of insulator geometry. For the purposes of this illustration, the electrokinetic movement ($\vec{F}_{EK}$) for all the channels is from left to right. For (A) and (B) the blue spheres represent a single population of identical particles of interest experiencing nDEP. (A) Typical g-iDEP behavior, where some analytes are trapped near point of greatest constriction at larger pitches before complete full cross section sequestration occurs. (B) Identical particles experience different outcomes depending on initial pathline. In some cases, particles on centerline can traverse gate, whereas those near the wall will be trapped. This results in like-particles being distributed throughout a range of gate pitches. (C) Near-centerline summation of forces for left-to-right $\vec{F}_{EK}$ and negative dielectrophoresis. (D) Various insulator shapes that are currently used that all allow variation in

like-particle behavior depending on initial pathline. Blue rectangles depict the point of strongest DEP interaction for a particle in a DC field.

For all iDEP designs, the constriction geometry defines the overall performance, whether the basic shape is repeated or varies some characteristic dimension. The assessment here focuses on the constriction design, which is universal to all iDEP systems.[15]. Examples of insulator shapes currently utilized include rectangle[14,27], triangle[21], sawtooth[11, 16, 28, 29], circular posts[10, 19, 25], and diamond posts.[19, 30] Trapping DEP leads to the isolation and concentration of analytes near the constriction points in the microchannels[1, 3, 8, 10, 11, 19, 25]. Separation can be achieved as a bipurification, where one analyte is trapped and other analytes continue to flow through the microchannel[10], or multiple analytes can be trapped in the same microchannel.[11] Separation can also be achieved using DEP using deflection techniques.[13, 31] Separation is possible in this case as the different mobilities of analytes results in different degrees of deflection when the particle passes the point of constriction in the microdevice.[32] Inducing the same behavior for a given particle type across all starting points will improve all existing iDEP systems.

Each of these configurations creates different local environments for the analytes relative to the local longitudinal axis dependent upon the initial lateral position in the channel (Figure 1).[1, 33, 34] This is true for local traps or elution strategies. For the purpose of high resolution separations, several factors come into play; including high values for the electric field and gradient[12] and the induction of all particles of an identical population to traverse the longitudinal axis in a similar fashion where the electric field strength and gradient intensity achieve separatory differentials (whether trapping, streaming (multi-outlet), or stochastic-based and chromatography-like elution-based strategies).[10, 11, 28, 29, 35-39] The identical or at least similar (accounting for diffusion and dispersion) movement of all particles of an identical population is a core tenet of separations science. The manipulation of analytes by DEP is possible because each

analyte has unique properties reflected by their electrophoretic (μ_{EP}) and dielectrophoretic (μ_{DEP}) mobilities. For all microchannels changing the constriction size, shape of the insulator, suspending medium, or the applied potential will alter the particles interaction with microchannel.[3, 29, 40]

This work seeks to develop a novel insulator geometry to improve the separation capabilities of iDEP. By iteratively modeling current and potential new designs using finite element software, where a new multi-length scale insulator has been developed. The insulator design will streamline the particles, minimize the possibility for extraneous trapping zones, laterally homogenize the forces, while maintaining high gradients to allow for separation.

Theory

Manipulation of the analytes is possible because of the influence of the EK and the DEP forces. Further development can be found in several previous work.[9, 10, 19, 41, 42]

The electrokinetic velocity, $\vec{v}_{EK}$, is the combination of electrophoretic and electroosmotic velocities

$$\vec{v}_{EK} = \mu_{EK}\vec{E} = (\mu_{EOF} + \mu_{EP})\vec{E} \quad (1)$$

The DEP velocity, $\vec{v}_{DEP}$, can be represented in terms of dielectrophoretic mobility (μ_{DEP}) and the gradient of the electric field squared, $\nabla \left| \vec{E} \right|^2$.[41, 43, 44]

$$\vec{v}_{DEP} = \mu_{DEP}\nabla \left| \vec{E} \right|^2 \quad (2)$$

DEP is the force that is exerted on a polarizable spherical particle present in a non-uniform electric field.[41, 44]

$$\vec{F}_{DEP} = 2\pi\varepsilon_m r^3 f_{CM}\nabla \left| \vec{E} \right|^2 \quad (3)$$

where $\vec{F}_{DEP}$ is the DEP force, ε_m is the permittivity of the medium, r is the radius of the particle, and f_{CM} is the Clausius-Mossotti factor which is dependent on the conductivity of the particle and medium in DC fields. Depending upon the sign of f_{CM}, the particle of interest will either undergo positive or negative DEP. In positive DEP, the conductivity of the particle is greater than the conductivity of the media; meaning that the particle is attracted to areas of high electric field. In negative DEP, the conductivity of the media is larger than that of the particle so the particle is effectively repelled from the locations of high electric field strength.

The flow of analytes in a microfluidic channel is controlled by advection, diffusion and electrokinetic effects. [30] By eliminating pressure driven flow in the system advection can be ignored. For large particles (>1 μm) diffusion can be disregarded. Therefore particle flow, $\vec{j}$, can be described by the following[45,46]:

$$\vec{j} = D\nabla \mathrm{C} + C(\vec{v}_{Bulk} + \vec{v}_{EK} + \vec{v}_{DEP}) \approx C(\vec{v}_{EK} + \vec{v}_{DEP}) \quad (4)$$

Where *D* is the diffusion coefficient, *C* is the particle concentration, and $\vec{v}_{Bulk}$ is the motion of the fluid due to pressure driven flow. Therefore, particle flow is consequently only affected by the concentration of the analyte, EK, and DEP.

Dielectrophoretic forces are influenced by constrictions in the microchannel, as this is where the highest gradients are induced. Particle motion can be mostly attributed to EK when the particles are not at points of constriction in the microfluidic device, hence particle flow can be approximated by the electric field lines (Eq. 4).

Trapping of analytes occurs when the particle velocity along the field line is zero, $\vec{j} \cdot \vec{E} = 0$, such that $\vec{v}_{DEP}$is equal to $\vec{v}_{EK}$. Trapping of analytes can therefore be described using the EK and DEP mobilities:

$$\left(\mu_{EK} E + \mu_{DEP} \nabla \left|\vec{E}\right|^2\right) \cdot \vec{E} > 0 \quad (5)$$

Eq. 7 can be rearranged such that dielectrophoretic trapping is described as[47]:

$$\frac{\nabla|\vec{E}|^2}{E^2} \cdot \vec{E} \geq \frac{\mu_{EK}}{\mu_{DEP}} \tag{6}$$

For streaming and sorting DEP the threshold for trapping is never achieved, but the particles are influenced by DEP (Eq. 4).

EK and DEP result in extremely complex systems, however the behavior can be classified as either streaming or trapping behaviors. Trapping behaviors occur when the interaction between the $\vec{E}$ and the slope of $\frac{\nabla|\vec{E}|^2}{E^2} \cdot \vec{E}$ meet at highly acute angles. Streaming DEP occurs where the $\vec{E}$ and the slope of $\frac{\nabla|\vec{E}|^2}{E^2} \cdot \vec{E}$ interact at glancing angles.

Mathematical Modeling

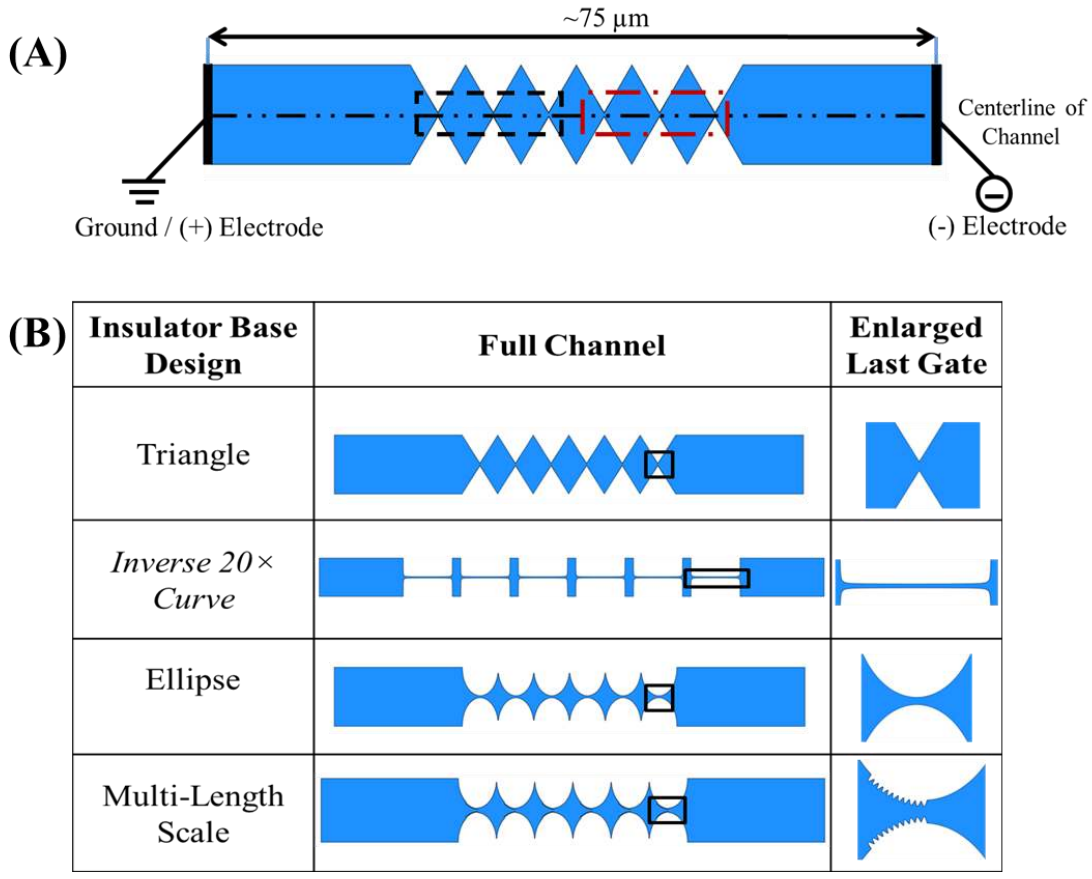

Figure 2. Illustration of generalized form of channels investigated computationally. (A) Enlarged sample schematic for one of the iDEP devices modeled. The approximate length of the channel and the constrictions were consistent for all models. The gate pitch of the first three gates is 36.37 µm and 34.10 µm for the second set of three gates. The only exception is for the *Inverse 20× Curve* where the channel was about 120 µm long. (B) Schematics of the some of the various insulator shapes and an enlarged view of the last gate. Other insulator shapes can be found in Supplementary Information.

Microchannel Geometries

For our system, six constriction microchannels with various insulators were used in this study; where the gate pitch changed after 3 gates, resulting in 2 gate groupings. The gate pitches were 36.37 µm and 34.10 µm (Figure 2A). The gate pitches were chosen to mimic measurements for a current channel design. The current channel measurements have been used for the manipulation and separation of several analytes including: polystyrene spheres, red blood cells,

different serotypes of *Escherichia coli*, and different strains of *Staphylococcus epidermidis*.[1, 8, 11, 28] The channels modeled ranged in length from 75-120 µm (only the *Inverse 20× Curve* channels were on the upper end of this). A 500 V potential was applied so that the inlet wall was a ground and the outlet wall carried the potential (Figure 2A). AutoCAD 2014 (Autodesk, Inc, San Rafael, CA) was used to build the to-scale microchannels.

Insulator geometries were modeled to determine their effects on the applied electric potential. The insulator geometries focused on the following features: the effect of sharp features (triangular shape), flat designs (*Inverse 20× Curve* and rectangular insulators), rounded insulators (circular and elliptical shapes), and the addition of small insulator features to larger geometry elements near or at the point of highest constriction (Figure 2B). Several other designs were studied; examples of these different geometries can be found in the Supplementary Material (Figure S1 & S2).

Finite Element Multiphysics Mathematical Models

The distribution of the electric potential was modeled using the finite-element multiphysics simulation software (COMSOL Multiphysics 5.1). The *AC/DC module* was specifically used to determine the distribution of the $\vec{E}$, $\nabla\left|\vec{E}\right|^2$, and $\frac{\nabla|\vec{E}|^2}{E^2}\cdot\vec{E}$.

Two dimensional models of the microchannels were utilized as the electric potential is expected to vary minimally across the channel depth as the channels are relatively shallow compared to the other dimensions of the microchannel.[47] The insulating posts will distort the electric field of the entire depth of the microchannel as they are they full height of the microchannel. The same material properties and element size parameters were used for all

microchannels for original comparison. The mesh was refined further for all designs developed in this paper.

The distribution of the electric potential in all microchannels was determined using the Laplace equation, where the electric potential (φ) within a microchannel is continuous:

$$\nabla^2\varphi = 0 \tag{7}$$

The boundaries are defined as the surfaces of the microchannel and insulators where the boundary conditions applied are as follows:

$$\vec{n} \cdot \vec{J} = 0 \text{ at the boundaries} \tag{8}$$

$$\varphi = V_{inlet} \tag{9}$$

$$\varphi = V_{outlet} \tag{10}$$

where $\vec{n}$ is the normal vector from the surface, $\vec{J}$ is the electrical current density, and V_{inlet} and V_{outlet} are the potentials applied at the inlet and outlet of the microchannel.

Results and Discussion

The shape of insulators in iDEP is the defining attribute towards the ability to manipulate analytes within a microfluidic channel. The insulator induces the distribution of $\vec{E}$ and therefore the $\nabla \left| \vec{E} \right|^2$ and the streaming or trapping of the analyte. For trapping, streaming, and sorting it is desirable for each particle of a given physical makeup to experience the same environment to ensure consistent outcomes. Dielectrophoretic forces must be high enough to overcome transport and diffusional forces to generate an observable effect. This requires large gradients, resulting in large $\nabla \left| \vec{E} \right|^2$ values. [1,12]

Depending on the geometric configuration and strength of the various forces, streaming or trapping can result. Sorting of particles in a continuous or semi-continuous mode has been an

important use of dielectrophoresis. A common strategy is deflection using streaming DEP, but recent work has shown sorting by exploiting trapping or trapping-like mechanisms. For deflection techniques to operate most efficiently, similar principles apply, in that, all particles of a population should occupy a homogenous environment during the deflection process. This suggests that each particle is influenced by the same $\frac{\nabla|\vec{E}|^2}{E^2} \cdot \vec{E}$ value at each point in the process.

The two features can be at odds with one another, by definition gradient means a change in the value and homegeneous suggest a consistent level. This study probes a large variety of insulator shapes to create an environment where high gradient values are attained, while giving a homogeneous environment to all particles exposed to the separatory system.

The following geometric constructs were probed. The effect of different base insulators: triangle, rectangle, *Inverse 20× Curve*, circle, and ellipse (Figure 3). Futhermore the addition of small insulators to the base structure was tested; variables included the shape of the small insulator(s) (triangle, ellipse, rectangle, and curved fin), number of small insulator(s), location on the base insulator (across the whole top or half, insetting the insulators in the base insulator), and height (diminishing insulator height). Examples of these different tested geometries can be found in the Supplimentary Information (Figure S2). All of these geometries were eliminated based on the following factors: not achieving high enough $\nabla \left| \vec{E} \right|^2$, inefficient streaming (presence of local traps) of analytes, and/or severe lateral field inhomogeniety.

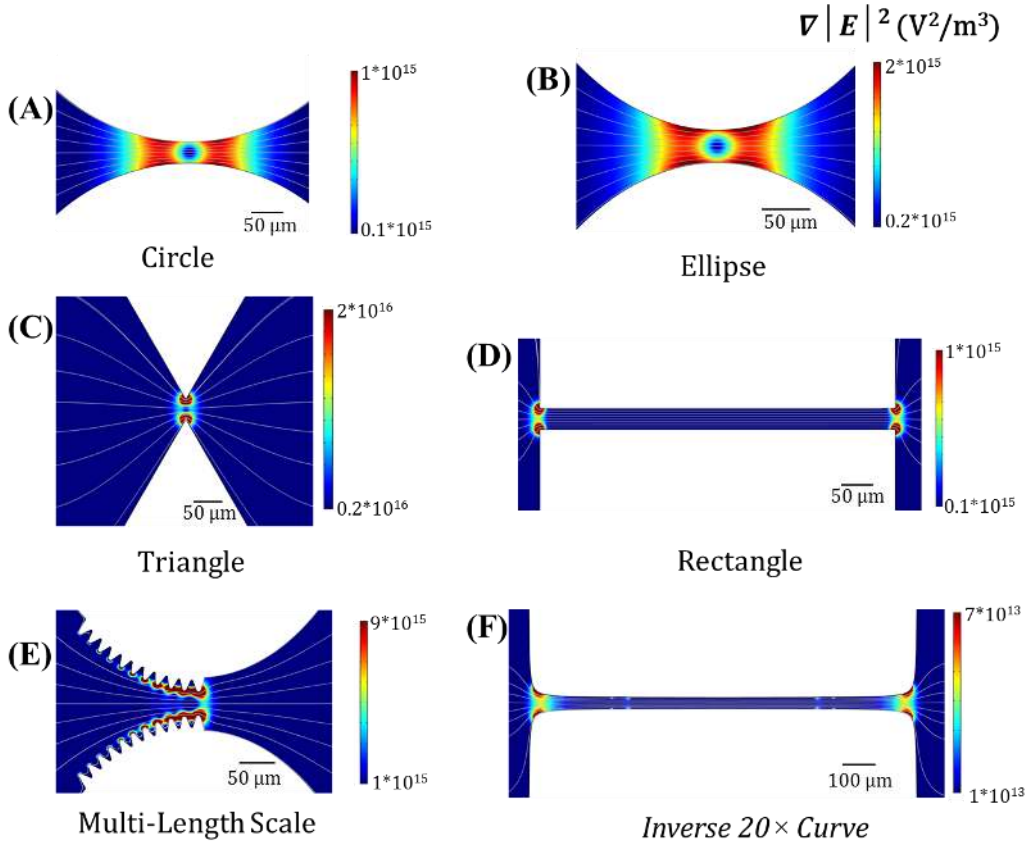

Figure 3. Study of general design options (others shown in Supplemental Material, Figure S2). Two dimensional plots of the $\nabla \left| \vec{E} \right|^2$ for different insulator shapes with electric field lines (grey). The absolute value for the color scale for each design is different to highlight the patterns that result from the specific insulator shape. Each image is of the first gate of 34.10 µm for the different designs.

To achieve high $\nabla \left| \vec{E} \right|^2$ the most effective insulator design has sharp points, demonstrated by the triangular insulator (Figure 3C). The radius of curvature for sharp features changes rapidly which, in turn, constricts the electric field and results in a high $\nabla \left| \vec{E} \right|^2$. The triangular insulator is representative of diamonds, sawteeth, and triangles used for insulators.[11, 16, 19, 21, 28-30] Along the centerline, the value for the gradient of the $\nabla \left| \vec{E} \right|^2$ is for the 34.10 µm gate is approximated to be 3.2×10^{16} V^2/m^3, which is the highest value of any of the insulator shapes examined. Particles will travel along the field line by EK forces in the absence of a significant gradient. However, these sharp features create local dielectrophoretic traps where the electric

field line impinges the slope of the local gradient at an acute angle. This is seen at the lateral pathlines away from the centerline for these triangle designs, which are representative of this class of insulator shapes. In cases where trapping does not occur, particles are deflected in a highly non-linear fashion preventing consistent separations via deflection and streaming.

Circular insulators have smaller gradients (Figure 3 A&B) as the constriction of the electric field is more gradual as compared to triangular insulators. Therefore only smaller $\nabla \left| \vec{E} \right|^2$ values are possible with the same constriction size compared to sharp insulators. The $\nabla \left| \vec{E} \right|^2$ along the centerline is 8.8×10^{14} and 1.85×10^{15} V^2/m^3 for the circular and ellipse shaped insulators respectively with a gate pitch of 34.10 µm.

Rectangular insulators are also used to alter the gradient of the electric field (Figure 3D).[14, 27] The maximum $\nabla \left| \vec{E} \right|^2$ along the centerline is 6.3×10^{14} V^2/m^3 with a gate pitch of 34.10 µm. The gradient for rectangular and *Inverse 20× Curve* insulators (Figure 3 D&F) are smaller than for circular and triangular insulators as the constriction of the electric field is abrupt, so a high gradient is limited to the corners of the insulators. These values are the lowest of any insulator shape, this could be increased by shortening the insulator or channel, however the $\nabla \left| \vec{E} \right|^2$ will still be lower than the other designs; leading to less influence on the particles in the channel.

The $\nabla \left| \vec{E} \right|^2$ is not the same laterally for the triangular, circular, and rectangular insulators, so that particles will experience different forces based on their initial pathlines. Within each of these designs, particles starting at various vertical positions (as drawn, lateral position relative to the longitudinal axis of the device and applied external electric field) will be trapped at widely varying locations (Figure 1); meaning that trapping DEP will not occur at the same voltage for the different analyte pathlines.[33, 34] The rectangular and *Inverse 20× Curve* have

the most laterally homogeneous electric field, however they do not have a strong enough gradient to trap analytes of typical interest.[12] For the case of sorting DEP methods having a low $\nabla \left| \vec{E} \right|^2$ will result in lower resolution separations as particles will not be deflected as much. This is compounded by the fact that like-particles along different pathlines will experience different forces, altering their deflection and thus the resolution of the separation. Streaming DEP is also affected as by having low $\nabla \left| \vec{E} \right|^2$ values, and thus lower DEP forces, the particles are not as effectively streamlined.

The advantage to multi-length scale design is the small insulators alter the distribution of the electric field significantly at the points approaching the constriction resulting in higher values for the $\nabla \left| \vec{E} \right|^2$, while the elliptical base creates a more homogenous lateral field. As the particles approach the point of constriction, under conditions of negative DEP, the analytes are pushed towards the center of the microchannel as they are repelled from the small insulators. The most useful insulator design from this study has an elliptically-shaped base insulator and small 20 μm elliptically-shaped insulators across half the top of the base (Figure 3E). The $\nabla \left| \vec{E} \right|^2$at the 34.10 μm gate pitch is 1.7×10^{15} V^2/m^3. This value is lower than for the triangular insulators, but higher than any of the other insulators.

All further comparisons made are between triangular insulator and the new multi-length scale insulator. The triangular insulator represents issues of partial trapping and an inhomogeneous lateral environment present for all other designs (circle and rectangle) and has the highest $\nabla \left| \vec{E} \right|^2$along the centerline. Using the definition of trapping in an iDEP device defined in Eq.4 particles are trapped based on the ratio of the μ_{EK} and μ_{DEP}. Using a known analyte (*Escherichia coli*), an established value for μ_{EK} is -1.0×10^{-8} m^2/Vs[8] and the

dielectrophoretic mobility can be calculated assuming the particle is between 0.1-1.0 μm, using the following relationship[12]:

$$\mu_{DEP} = \frac{\varepsilon_m r^2 f_{CM}}{3\eta} \quad (12)$$

where media permittivity (ε_m) is 10^{-9} F/m, the radius of the particle (r) is 10^{-6} to10^{-7} m, f_{CM} is -0.3, and solution viscosity (η) is 10^{-3}Ns/m^2.[12] This gives a range for μ_{DEP} of -1.0×10^{-17} to -1.0×10^{-19} m^4/V^{2}s. Therefore assuming a median value for μ_{DEP} of -1.0×10^{-18} m^4/V^{2}s, the ratio of the mobilities is 1×10^{10} V/m^2. This value reasonably coincides with the value determined for *Staphylococcus epidermidis* of 4.6 ± 0.6×10^9 V/m^2 for gentamicin resistant and 9.2 ± 0.4×10^9 V/m^2 for gentamicin sensitive.[11]

A direct visual 2D comparison of $\frac{\nabla|\vec{E}|^2}{E^2} \cdot \vec{E}$ within the two designs provides evidence for significantly different behaviors (Figure 4). In these representations, the intensity of the $\frac{\nabla|\vec{E}|^2}{E^2} \cdot \vec{E}$ value is plotted showing effect on a particle with a mobilities ratio of 1×10^{10} V/m^2. The design was created to show, at the specified ratio, trapping behavior at slightly narrower gate (right) and complete passage of all particles at the wider gate (left) for the multi-length scale design (Figures 4B and 4D). Plots emphasizing electric field lines are included (Figures 4C & 4D) in this visual study. The color scale toward red is the most repelling environment and the white areas completely exclude analytes with these properties. The portions with color define the area accessible to this analyte. This can be observed by noting that the white area completely bridges the gap on the right gate, indicating excluded area and trapping behavior.

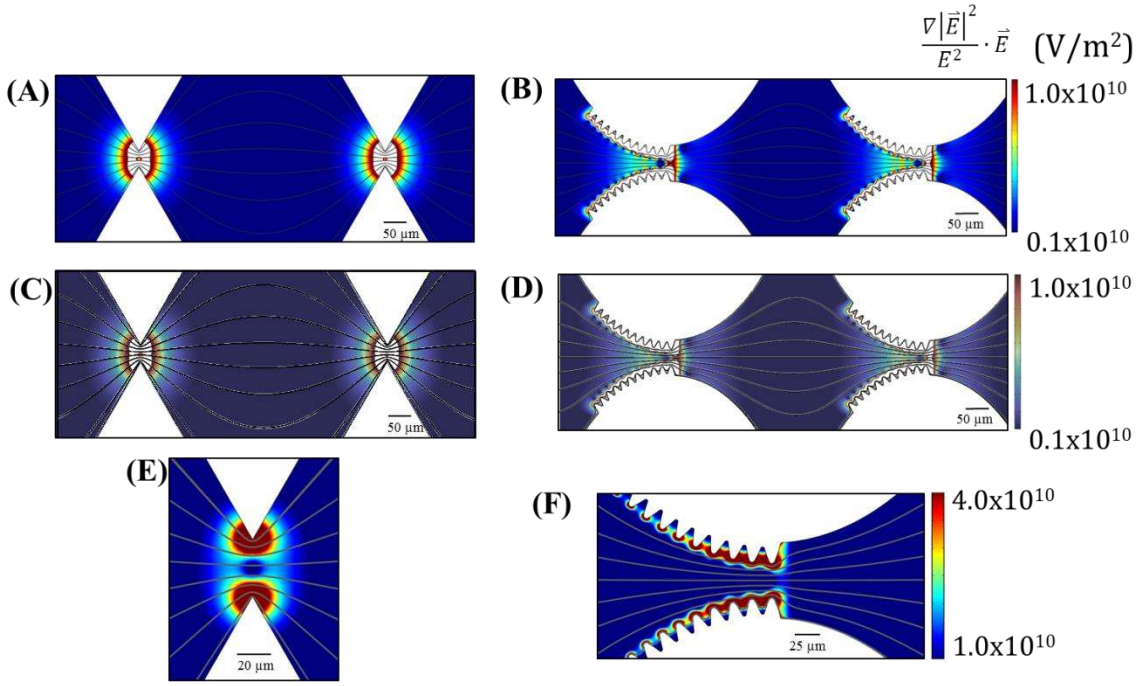

Figure 4. Study emphasizing differences between triangular and multi-length scale insulators at the critical transition to full trapping at second gate (non-trapping at left, trapping at right, panels B & D). Similar data is shown in all six panels, with different representations to emphasize various transport and trapping features. Panels A-D shows the area that is accessible, the colored region, to a particle that would be repelled (nDEP) with a given particle property of (μ_{EK}/μ_{DEP} =1×10^{10} V/m^2). Panels E & F show the full distribution of $\frac{\nabla|\vec{E}|^2}{E^2}\cdot\vec{E}$ for the 34.10 um gate. Electric field lines present in all panels, emphasized in panels C & D. At low $\frac{\nabla|\vec{E}|^2}{E^2}\cdot\vec{E}$ values, electric field lines are the pathlines of particles. Panels showing triangular insulator (A, C, & E) show electric field lines off the centerline impinging the slope of the $\frac{\nabla|\vec{E}|^2}{E^2}\cdot\vec{E}$ (local direction of dielectrophoretic forces) at highly acute, creating a local trapping point. These lateral trapping areas are present at all sharp features and some rounded features (Figure 3 and Supplemental Information). In this study, for the triangular insulator given the analyte μ_{EK}/μ_{DEP} ratio of choice, the analyte is fully trapped at both gates. In contrast, the critical particle would pass the first gate completely and be trapped at the second gate for the multi-length scale insulator. Further, the multi-length scale insulator does not exhibit any lateral traps were the electric field lines impinge the $\frac{\nabla|\vec{E}|^2}{E^2}\cdot\vec{E}$ slope at extremely acute angles. The $\frac{\nabla|\vec{E}|^2}{E^2}\cdot\vec{E}$ scale is the same for each pair of images (A-F). The gate pitches are 36.37 µm and 34.10µm, left to right (A-D).

Significantly different behaviors can be deduced for the triangular insulators (Figures 4A, 4C & 4E). It is important to note before further discussion that a mobilities ratio could be presented that allows for passage of particles along the centerline of the wider gate (left) and trap

at the smaller gate (left) for this insulator type. However and very importantly, all of the particles could not traverse the larger gate under these conditions. For particles off the centerline, the electrokinetic pathlines impinge upon the gradient at an acute angle, allowing for partial trapping at the wider gate. This is especially apparent for the enlarged tip area with all the $\frac{\nabla|\vec{E}|^2}{E^2}\cdot\vec{E}$ values within the color scale (Figure 4E). At the top (or bottom) the pathlines clearly impinge on the slope of the $\frac{\nabla|\vec{E}|^2}{E^2}\cdot\vec{E}$ at an acute angle. When full trapping across the gate occurs, an arc forms represented by the left edge of the white areas (Figures 4 A & 4C). This arc structure has been observed in many experimental systems.[33, 34] The net result is consistent with current experimental systems, where small collections of analytes are observed at the tips of wide gates and full arcs form when complete trapping across the lateral dimension occurs. For a single particle population, some particles will trap on these wide gate tips, while other will continue on which distributes that single population throughout the device.

The reason the multi-length scale system prevents these local traps at wide gates is the slope of the $\frac{\nabla|\vec{E}|^2}{E^2}\cdot\vec{E}$ impinges upon the electrokinetic lines at a glancing angles and simply streams the particles toward the centerline. If the centerline trapping forces are insufficient, no trapping occurs at that gate.

One feature which promises improved results beyond the removal of local traps is that the assessable area limits the lateral variation in $\frac{\nabla|\vec{E}|^2}{E^2}\cdot\vec{E}$. At a trapping point (white area bridging the gap), the values are relatively constant across the entire gap, at least an order of magnitude smaller than the triangular insulator design (Supplemental Information Figure S3). This is a direct result of the particles being constrained to the fifteen or so microns in the center of the

34.10 μm gap (Figure 4F). Plots investigating the quantitative nature of the lateral heterogeneity of the various insulator designs were fully investigated (Supplemental Information).

For sorting and streaming techniques the forces are more uniform laterally with the multi-length scale insulator meaning that the particles will be repelled or deflected in more similar manners. This will ultimately lead to higher resolution separations as particles are deflected the same amount and better streaming will occur as the particles will be confined to a smaller area in the channel than with the other designs.

Conclusion

The development of a new multi-length scale insulator for iDEP will allow for improved separations for both deflection and trapping techniques. The new insulator will streamline the analytes to ensure that like-particles experience similar environments as the $\overrightarrow{E}$ is more homogenous in the accessible area. Furthermore, the minimization of partial and extraneous trapping should be possible. This can all be accomplished while maintaining $\frac{\nabla|\vec{E}|^2}{E^2} \cdot \vec{E}$ values high enough to accomplish trapping.

References

[1] Jones, P. V., Staton, S. J. R., Hayes, M. A., *Anal. Bioanal. Chem.* **2011**, *401*, 2103-2111.
[2] Luo, J., Abdallah, B. G., Wolken, G. G., Arriaga, E. A., Ros, A., *BIOMGB* **2014**, *8*, 021801.
[3] Staton, S. J. R., Jones, P. V., Ku, G., Gilman, S. D., Kheterpal, I., Hayes, M. A., *Analyst* **2012**, *137*, 3227-3229.
[4] Nakano, A., Camacho-Alanis, F., Ros, A., *Analyst* **2015**, *140*, 860-868.
[5] Washizu, M., Kurosawa, O., *IEEE Transactions on Industry Applications* **1990**, *26*, 1165-1172.
[6] Chou, C.-F., Tegenfeldt, J. O., Bakajin, O., Chan, S. S., Cox, E. C., Darnton, N., Duke, T., Austin, R. H., *Biophys. J.* **2002**, *83*, 2170-2179.
[7] Martinez-Duarte, R., Camacho-Alanis, F., Renaud, P., Ros, A., *Electrophoresis* **2013**, *34*, 1113-1122.
[8] Jones, P. V., DeMichele, A. F., Kemp, L., Hayes, M. A., *Anal. and Bioanal. Chem.* **2014**, *406*, 183-192.

[9] Lapizco-Encinas, B. H., Simmons, B. A., Cummings, E. B., Fintschenko, Y., *Anal. Chem.* **2004**, *76*, 1571-1579.
[10] Lapizco-Encinas, B. H., Simmons, B. A., Cummings, E. B., Fintschenko, Y., *Electrophoresis* **2004**, *25*, 1695-1704.
[11] Jones, P. V., Huey, S., Davis, P., McLemore, R., McLaren, A., Hayes, M. A., *Analyst* **2015**, *140*, 5152-5161.
[12] Jones, P. V., Hayes, M. A., *Electrophoresis* **2015**, *36*, 1098-1106.
[13] Abdallah, B. G., Chao, T.-C., Kupitz, C., Fromme, P., Ros, A., *ACS Nano* **2013**, *7*, 9129-9137.
[14] Srivastava, S. K., Baylon-Cardiel, J. L., Lapizco-Encinas, B. H., Minerick, A. R., *J. Chromatogr. A* **2011**, *1218*, 1780-1789.
[15] Srivastava, S., Gencoglu, A., Minerick, A., *Anal Bioanal. Chem.* **2011**, *399*, 301-321.
[16] Chen, K. P., Pacheco, J. R., Hayes, M. A., Staton, S. J. R., *Electrophoresis* **2009**, *30*, 1441-1448.
[17] Gencoglu, A., Minerick, A., *Lab Chip* **2009**, *9*, 1866-1873.
[18] Pohl, H. A., *J. Appl.Phys.* **1951**, *22*, 869-871.
[19] Cummings, E. B., Singh, A. K., *Ana.l Chem.* **2003**, *75*, 4724-4731.
[20] Keshavamurthy, S. S., Leonard, K. M., Burgess, S. C., Minerick, A. R., *NSTI-Nanotech, Boston, MA* **2008**, 401-404.
[21] Kang, Y., Li, D., Kalams, S., Eid, J., *Biomed. Microdevices* **200**8, *10*, 243-249.
[22] Barbulovic-Nad, I., Xuan, X., Lee, J. S. H., Li, D., *Lab Chip* **2006**, *6*, 274-279.
[23] Thwar, P. K., Linderman, J. J., Burns, M. A., *Electrophoresis* **2007**, *28*, 4572-4581.
[24] Lapizco-Encinas, B. H., Davalos, R. V., Simmons, B. A., Cummings, E. B., Fintschenko, Y., *J. Microbiol. Methods* **2005**, *62*, 317-326.
[25] Sabounchi, P., Morales, A., Ponce, P., Lee, L., Simmons, B., Davalos, R., *Biomed. Microdevices* **2008**, *10*, 661-670.
[26] Regtmeier, J., Duong, T. T., Eichhorn, R., Anselmetti, D., Ros, A., *Anal. Chem.* **2007**, *79*, 3925-3932.
[27] Kang, K. H., Kang, Y., Xuan, X., Li, D., *Electrophoresis* **2006**, *27*, 694-702.
[28] Staton, S. J. R., Chen, K. P., Taylor, T. J., Pacheco, J. R., Hayes, M. A., *Electrophoresis* **2010**, *31*, 3634-3641.
[29] Pysher, M. D., Hayes, M. A., *Anal. Chem.* **2007**, *79*, 4552-4557.
[30] LaLonde, A., Gencoglu, A., Romero-Creel, M. F., Koppula, K. S., Lapizco-Encinas, B. H., *J. Chromatogr. A* **2014**, *1344*, 99-108.
[31] Srivastava, S. K., Artemiou, A., Minerick, A. R., *Electrophoresis* **2011**, *32*, 2530-2540.
[32] Abdallah, B. G., Roy-Chowdhury, S., Coe, J., Fromme, P., Ros, A., *Anal. Chem.* **2015**, *87*, 4159-4167.
[33] Gallo-Villanueva, R. C., Sano, M. B., Lapizco-Encinas, B. H., Davalos, R. V., *Electrophoresis* **2014**, *35*, 352-361.
[34] Saucedo-Espinosa, M. A., Lapizco-Encinas, B. H., *Electrophoresis* **2015**, *36*, 1086-1097.
[35] Giddings, J. C., *Unified Separation Science*, John Wiley & Sons, Inc., New York **1991**.
[36] Morton, K. J., Loutherback, K., Inglis, D. W., Tsui, O. K., Sturm, J. C., Chou, S. Y., Austin, R. H., *Proc. Natl. Acad. Sci.U.S.A* **2008**, *105*, 7434-7438.
[37] Huang, L. R., Cox, E. C., Austin, R. H., Sturm, J. C., *Science* **2004**, *304*, 987-990.
[38] Streek, M., Schmid, F., Duong, T. T., Ros, A., *J. Biotechnol.* **2004**, *112*, 79-89.

[39] Ros, A., Hellmich, W., Regtmeier, J., Duong, T. T., Anselmetti, D., *Electrophoresis* **2006**, *27*, 2651-2658.
[40] Ozuna-Chacón, S., Lapizco-Encinas, B. H., Rito-Palomares, M., Martínez-Chapa, S. O., Reyes-Betanzo, C., *Electrophoresis* **2008**, *29*, 3115-3122.
[41] Pohl, H. A., *Dielectrophoresis : the behavior of neutral matter in nonuniform electric fields* Cambridge University Press, Cambridge; New York 1978.
[42] Pethig, R., *BIOMGB* **2010**, *4*, 022811.
[43] Probstein, R. F., *Physicochemical Hydrodynamics: An Introduction*, John Wiley & Sons, Inc. **1994**, pp 1-8.
[44] Jones, T. B., *Electromechanics of Particles*, Cambridge University Press, 1995.
[45] Cummings, E. B., *Engineering in Medicine and Biology Magazine, IEEE* **2003**, *22*, 75-84.
[46] Kwon, J.-S., Maeng, J.-S., Chun, M.-S., Song, S., *Microfluid. Nanofluid.* **2008**, *5*, 23-31.
[47] Baylon-Cardiel, J. L., Lapizco-Encinas, B. H., Reyes-Betanzo, C., Chavez-Santoscoy, A. V., Martinez-Chapa, S. O., *Lab Chip* **2009**, *9*, 2896-2901.

Acknowledgements
This work was supported by National Institutes of Health grants 1R03AI094193-01, 1R03AI099740-01, and R03AI111361-01.

The authors declare no competing financial interest.

For Table of Contents Only